THE JOURNAL OF PHYSICAL CHEMISTRY C

C: Surfaces, Interfaces, Porous Materials, and Catalysis

Properties of NTCDA Thin Films on Ag(110): STM, Photoemission, NEXAFS and DFT Investigations

Yongfeng Tong, Javier Daniel Fuhr, Maria Luz Martiarena, Hamid Oughaddou, Hanna Enriquez, François Nicolas, Karine Chaouchi, Stefan Kubsky, and Azzedine Bendounan

J. Phys. Chem. C, **Just Accepted Manuscript** • DOI: 10.1021/acs.jpcc.8b08093 • Publication Date (Web): 12 Dec 2018

Properties of NTCDA Thin Films on Ag(110): STM, Photoemission, NEXAFS and DFT Investigations

Yongfeng Tong [1,2], Javier D. Fuhr[3], Maria Luz Martiarena [3], Hamid Oughaddou [2], Hanna Enriquez [2], François Nicolas [1], Karine Chaouchi[1], Stefan Kubsky [1] and Azzedine Bendounan [1,*]

[1] Synchrotron SOLEIL, L'Orme des Merisiers, Saint-Aubin – BP 48, F-91192, Gif-sur-Yvette Cedex, France
[2] Institut des Sciences Moléculaires d'Orsay, Université Paris-Sud, 91405 Orsay Cedex, France
[3] CONICET, Centro Atómica Bariloche Bustillo 9500 – 8400 Bariloche, Argentina
* Correspondence: azzedine.bendounan@synchrotron-soleil.fr; Tel.: +33-169-35-9799

Abstract: It is well proven that the properties of organic/metal interfaces play an upmost role in the performance of the organic devices. Here we present a study on structural and electronic properties of high quality 1,4,5,8-naphthalene tetracarboxylic dianhydrid (NTCDA) films grown on an Ag(110) surface. High-resolution scanning tunnelling microscopy (STM) and low energy electron diffraction (LEED) show the presence of two molecular domains. Density functional theory (DFT) calculations indicate that the most stable location of NTCDA corresponds to anhydride Oxygen attached to the Ag atoms along the [110] direction. Photoemission results of the C1s and O1s core levels demonstrate a strong interfacial bonding, inducing a charge transfer from the Ag metal to the molecular monolayer. An angular dependent study of the C K-edge near edge X-ray fine structure (NEXAFS) spectra provides detailed information concerning the evolution in the NTCDA orientation with the film thickness.

Keywords: Carbon; NTCDA, self-assembly, photoemission, STM, DFT, organic/metal interface

1. Introduction

Molecular architecture on metal surfaces represents an important issue in the exploration of nano-devices[1], where self-organization of organic molecules in well-defined geometries plays an essential role.[2,3] A fundamental aspect is the interaction at the metal-organic interface that significantly influences the self-assembly properties and thus determines the overall performance of the devices. Therefore, an understanding of this interaction is of paramount importance for optimizing the effectiveness of the organic components.[4] In other words, the performance of many electronic devices based on organic films such as organic field effect transistors (OFETs), organic light emitting devices (OLEDs) and Solar cells[5-9] depends on the bonding of the organic molecules to the metal surface[10] and this is why great attention has been paid to studying the properties of organic/metal interfaces by various experimental and theoretical tools.[11-14] Due to their planar structure, large π-conjugated aromatic organic molecules have the advantage to favor the self-assembly phenomenon on metal surfaces. In addition, such self-organized structures can induce overlapping between aromatic π-orbitals of adjacent molecules leading to delocalization of valence electrons within the molecular film.[15-17] In this context, a large number of studies of π-conjugated molecules like NTCDA,[18-21] PTCDA,[22-26] NTCDI,[27] PTCDI[28] and Pentacene[29,30] reveal a strong covalent hybridization between the molecules and the reactive metals, resulting in changes in the characteristics of the organic molecular orbitals. Such changes can substantially affect the physical properties of the film, like the electron mobility. In the present work, we have studied 1,4,5,8-naphthalene tetracarboxylic dianhydride (NTCDA) monolayer (ML) deposited on Ag(110)

substrate. The NTCDA molecule has D2h symmetry along the axis and consists of a naphthalene core with carboxyl and anhydride end groups. In the literature, it was reported that the core and the end groups participate both in the bonding of the molecule with the metal surfaces and play an essential role in determining the assembly of the molecules over the surface.[18] According to literature, NTCDA in the first ML lies flat with respect to the surface plane, mainly because of the strong interaction with the metal. However, in the case of multi-layer the NTCDA molecules tend to be inclined and give rise to a lamellar structure as that found in the bulk crystal structure. Similar results could be obtained when NTCDA was adsorbed on inert surfaces like sulfide, graphite, or pre-passivated substrates, where the intermolecular interaction exceeds molecule-substrate interaction.[31] On the other hand, it was observed that the NTCDA molecules are bonded to the metal surface via the carboxylic head-group due to the high electronegativity of the O atoms. An electron is transferred from the metal surface to fill the LUMO of the molecule, leaving a positive local state in the metal. This behavior leads to enhancing the chemical bonding between the oxygen and metal atoms and induces a bending of the NTCDA molecules with carboxylic head-group lying closer to the surface.[32,33] In the present paper, the properties of high-quality NTCDA films on Ag(110) surface were systematically analyzed using various techniques. We have chosen the NTCDA molecule because of its successful and promising applications in electronic devices, such as increasing the conversion efficiency of organic solar cells[34] and improving the electron mobility of OLEDs and of OFETs.[35] We extended our study to the Ag(110) substrate, which represents a reactive template for growing NTCDA film.[36] Our aim was in fact to revise the structure of the NTCDA monolayer system. In particular, low temperature scanning tunneling microscopy (LT-STM) was utilized to identify the two molecular domains as suggested from the low energy electron diffraction (LEED) patterns. Photoemission spectra of the core levels and of the valence band are presented in combination with near edge X-ray fine structure (NEXAFS) data to understand the chemical properties at the interface. In addition, the angular dependence of the NEXAFS spectrum provides information on the orientation characteristics of the NTCDA films.

2. Materials and Methods

2.1. Experiment

The photoemission experiments were carried out using a hemispherical Scienta SES 2002 electron energy analyzer at the TEMPO beamline of Synchrotron SOLEIL, France. The energy resolution of the analyzer depends on the pass energy (PE) and is estimated to be about 50 meV at high PE and 5 meV at low PE. Photoemission of the core levels and the valence band, together with NEXAFS measurements were performed using synchrotron radiation where the suitable photon energy can be chosen. Core level spectra of O1s and C1s were taken after deposition of NTCDA layer with different thicknesses. All the spectra were calibrated with $Au4f_{7/2}$ at a binding energy of 84 eV on a clean Au substrate. The valence band data were taken at hv=60 eV and calibrated with respect to the Fermi level. The NEXAFS spectra were carried out at the C1s and O1s K-edges by varying the angle Θ of the incoming beam with respect to the surface plane. The angle was varied from Θ=90° (with the electric field vector of the light parallel to the surface plane) to Θ=15° (nearly perpendicular to it). The NEXAFS spectra were also normalized with a reference adsorption spectrum measured on carbon-free and clean Au(111) surface under the same experimental conditions. Such a procedure permits to eliminate the effect of the carbon contamination present on

the optical mirrors of the beamline. All the photoemission experiments were conducted at room temperature. The STM and LEED measurements were performed using Omicron high resolution STM system. Both low and room temperature STM measurements have been carried out. The corresponding bias and tunnel current are indicated in the images, respectively. All measurements were performed under ultra-high vacuum of 10^{-10} mbar and the STM images were calibrated due to possible thermal drift during the scanning.

The NTCDA was purchased from Sigma-Aldrich without further purification. An Ag(110) single crystal was prepared with several cycles of standard sputtering with Ar^+ and annealing at high temperature until getting a good surface quality. The cleanliness was checked by core level photoemission and by analyzing the surface state band. Low energy electron diffraction (LEED) permitted to probe the surface crystallographic structure. The deposition of NTCDA was performed using a homemade evaporator, which has been degassed for several hours before the evaporation. The deposition flux was monitored by a quartz balance and the rate was estimated to about 1A/min. The preparation was conducted in an UHV chamber with base vacuum of $1x10^{-10}$ mbar.

The fitting procedure of the photoemission spectra was made after a proper Shirley background subtraction. We have used voigt peaks for the fitting of the photoemission spectra and the binding energy values are listed in Table 1.

2.1. Theory

The density functional theory (DFT) calculations have been carried out within the slab-supercell approach by using the Vienna *ab initio* simulation program (VASP).[37,38] The one-electron Kohn-Sham orbitals are expanded in a plane-wave basis set and electron-ion interactions are described through the PAW_PBE pseudo-potentials.[39,40] Exchange and correlation (XC) are described within the van der Waals density functional (vdW- DF)[41] with optB86b as exchange functional.[42] The sampling of the Brillouin zone is carried out according to the Monkhorst-Pack method.[43] The chosen cut-off energy is 400 eV, electron smearing is introduced following the Methfessel-Paxton technique[44] with σ = 0.2 eV and all the energies are extrapolated to 0 K. The convergence of the energy is kept always on the order of 10^{-4} eV. For each configuration we performed a full relaxation, except for the two bottom layer, while the forces are assured to be lower than 10^{-1} eV/nm.

For bulk Ag, by using a cut-off energy of 400 eV and a 16x16x16 k-point mesh we obtained a lattice parameter a_{Ag} of 4.097 Å. This result is in excellent agreement with the experimental value of 4.08 Å at room temperature. To obtain the single molecule geometrical configuration we calculated a full relaxation of all atom coordinates in a unit cell of 20 × 20× 20 $Å^3$ using a 1 × 1 × 1 k-point mesh. The monolayer of NTCDA molecules adsorbed onto a Ag(110) surface was studied considering a slab of six layers of Ag(110) in a unit cell with lattice parameters b_1 = (12.2914, 0.0, 0.00) Å and b_2 = (4.097, 8.691, 0.00) Å (|b|= 9,608 Å), using a 5 × 7 × 1 k-point mesh. The vacuum layer region between consecutive slabs is 17.8 Å, thick enough to ensure negligible interactions between periodic images normal to the surface when we include the layer.

The adsorption energy per molecule was calculated as:

$E_{ads} = -E(NTCDA/Ag(110)) + E(NTCDA) + E(Ag(110))$

Where *E(NTCDA/Ag(110))*, *E(NTCDA)* and *E(Ag(110))* are the total energy for *NTCDA/Ag(110)*, *NTCDA* and *Ag(110)* respectively.

We use the Bader method to calculate the charge around the atoms.[45] The Bader analysis has been done considering the total charge density (core plus valence charge density). The STM images were simulated within the Tersoff-Hamann approach[46] where the partial charge density is proportional to the tunneling current at the position of the STM tip. The simulated images correspond to constant current mode, using the same bias voltage than the experimental one, and an isodensity of 2.5x10^{-5} electrons/Å^3.

3. Results and discussion

3.1. STM and LEED investigations

Although the NTCDA/Ag(110) system has been already studied in the past by other techniques, one can however notice that STM imaging of its surface structure is still missing, whereas it exists for other substrates[47-49] and for analogue systems such as PTCDA on Ag(110).[50] Therefore, we would like here to discuss the structure of the NTCDA monolayer on Ag(110) through a combination of high-resolution STM images and low energy electron diffraction patterns.

Figure 1a,1b show room temperature STM images, in which large areas of two domains can be observed. The domains are clearly separated by molecular boundaries. All molecules in each domain are aligned in a row-like arrangement. STM image of one domain is displayed in Figure 1c, where the lattice of the Ag(110) surface is also observed, thanks to the good atomic resolution. Note that we observe different shapes of the molecules depending on the applied voltage, which is likely due to the fact that we probe different molecular orbitals. To gain a better understanding of the molecular arrangement, we extracted from the STM image both the base lattice of the Ag(110) substrate (Figure 1d) and that of the molecular monolayer. Some bright spots are also seen, which may be due to the diffusion of some NTCDA molecules, as observed in our previous work.[49] A comparison between the two lattices permitted to determine the angle between the molecular domains and the [1 -1 0] direction of Ag substrate to be about 28°.

The crystalline structure of the NTCDA monolayer on Ag(110) can be further analyzed by looking to the LEED pattern taken at 35eV shown in Figure 1e. The diffraction pattern confirms the existence of the two domains on the surface of one monolayer. Moreover, from the LEED pattern we obtained a superstructure matrix M=(3 0, 1 3) with respect to the Ag(110) unit cell with vectors $|\mathbf{a}_1|=a_{Ag}$, $|\mathbf{a}_2|=a_{Ag}/\sqrt{2}$, in perfect agreement with the simulation pattern shown in Figure 1f. The pattern was rotated by 20° to have a good comparison with the LEED image. It is worth noting that in the unit cell only one molecule was included, which is quite different from the one on Ag(100)[12] and Ag(111)[13] substrates. The unit cell obtained from the simulated pattern correspond to **b**1=12.6Å, **b**2=8.7Å and an angle Θ=76.7°. This unit cell area of 106.4 Å^2 is the same than the one reported in ref.[12]. However, the unit cell we obtain is different than the one reported in Figure 6c of ref.[12] and Fig. 1b of [51].

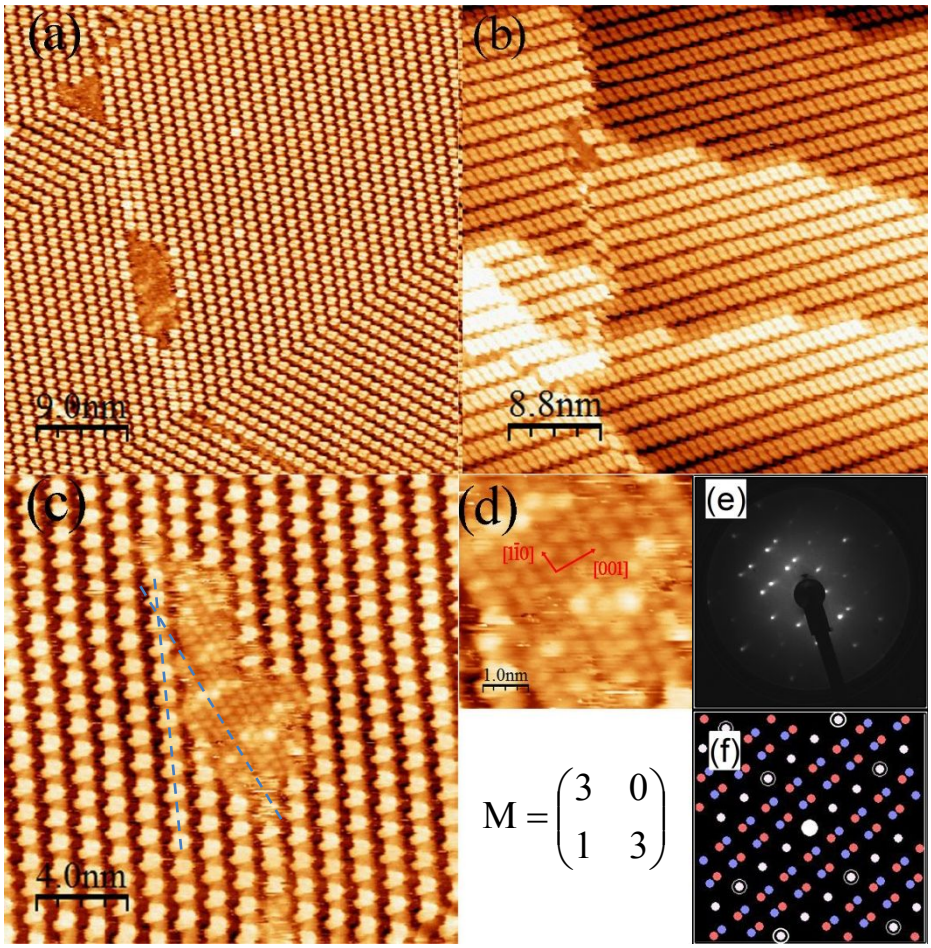

Figure 1: (a,b) Room temperature STM image of the NTCDA monolayer on Ag(110) surface at different scan conditions, (a) V=-0.24V, I=0.22nA and (b) V=-0.35V, I=0.22nA. (c) Reduced-scale image of one domain not completely covered where the atomic arrangement of the Ag(110) surface lattice is observed, V=0.55V, I=0.22nA. This lattice is marked in red in image (d). (e, f) LEED pattern and the corresponding simulation pattern that gives a structure described by the matrix M. In the simulation pattern, the red, blue and white dots refer to the diffraction spots by the surface lattices of the two molecular domains characterizing the NTCDA monolayer. The white dots represent an overlap of the red and blue dots. The white dots highlighted by circles refer also to the Ag(110) reciprocal lattice.

We performed DFT optimizations of a monolayer of NTCDA on Ag(110) for these two unit cells. Figure 2 show the two relaxed configurations: panel (a) correspond to the unit cell proposed here which have an adsorption energy of 2.89eV, while panel (b) corresponds to the unit cell of refs [12] and [51] which has an adsorption energy of 2.65 eV. We show also in Figure 2 the comparison, for each case, between the simulated LEED with the experimental one. We can see that the DFT calculations favour our proposed configuration, and the LEED comparison clearly rules out the previously proposed unit cell.

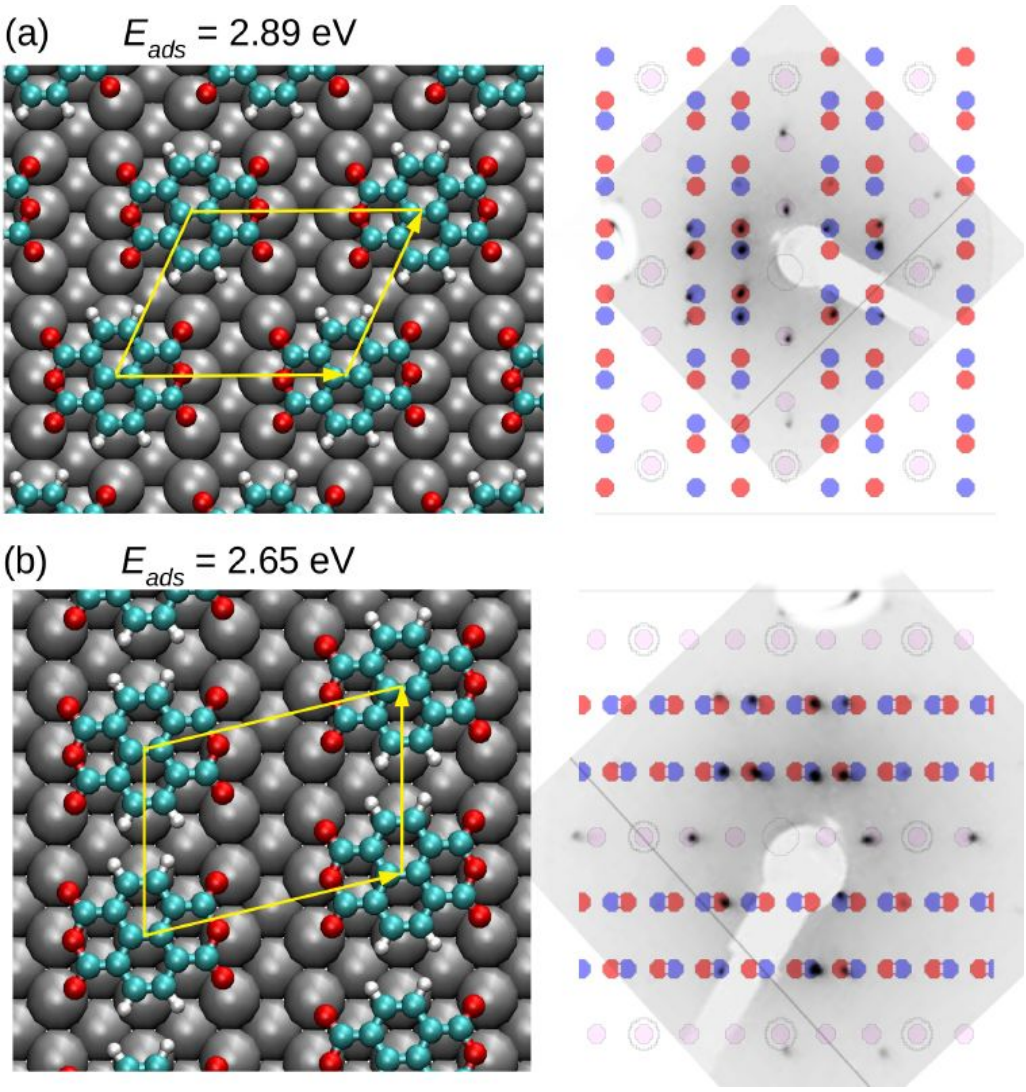

Figure 2: Optimized geometrical configurations of NTCDA/Ag(110), and the corresponding comparison of simulated and experimental LEED patterns: (a) this work unit cell. (b) unit cell previously proposed in Refs.[12] and [51]. In the simulation pattern, the red, blue and pink dots refer to the diffraction spots by the surface lattices of the two molecular domains characterizing the NTCDA monolayer. The pink dots represent an overlap of the red and blue dots. The pink dots highlighted by circles refer to the Ag(110) reciprocal lattice.

To obtain a more detailed description of the structural properties, high resolution low temperature STM images were taken and are shown in Figure 3(a,b). In panel (c) of Figure 3 we show the simulated STM images corresponding to the NTCDA monolayer on Ag(110) with V= 0.4V for the configuration described in Figure 2. From the STM images, it seems that the molecules in both domains are positioned with the same orientation and are aligned along the same direction as of the Ag(110) surface. For a better interpretation of the image, the NTCDA molecule has been superimposed on an enlarged experimental and simulated STM images (Figure 3d). This allows to determine the way how the molecules arrange within the rows with respect to the Ag(110) substrate.

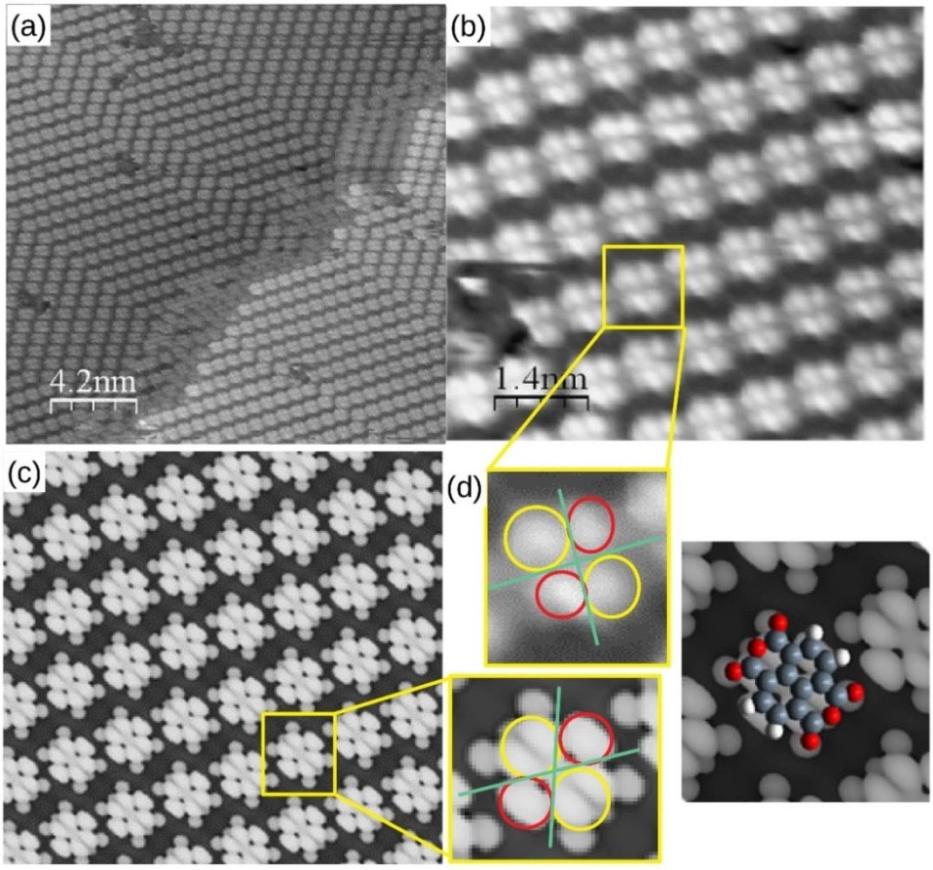

Figure 3: (a) Large scale of high resolution LT-STM of NTCDA monolayer on Ag(110). (V= 0.4V, I= 0.3nA). (b) Enlarged domain. (c) Simulated STM at voltage V=0.4V and at a distance between the tip and the molecule atoms of about 4Å. (d) Main features comparison between experimental and simulated images, and molecular arrangement with respect to STM image.

3.2. Core level photoemission

The XPS C1s and O1s core level spectra are displayed in Figure 4. The photon energy used was 360 eV for carbon and 700 eV for oxygen. No clear angular dependence was observed for neither C nor O, indicating the absence of out-of-plane orientation of the molecule in the monolayer regime. For a quantitative description of the different spectroscopic features, detailed de-convolution of the C1s and O1s features was given. The fitting procedure was conducted after a proper Shirley background subtraction. Strong constraint was applied to minimize the free parameters as has been mentioned in the experimental section.

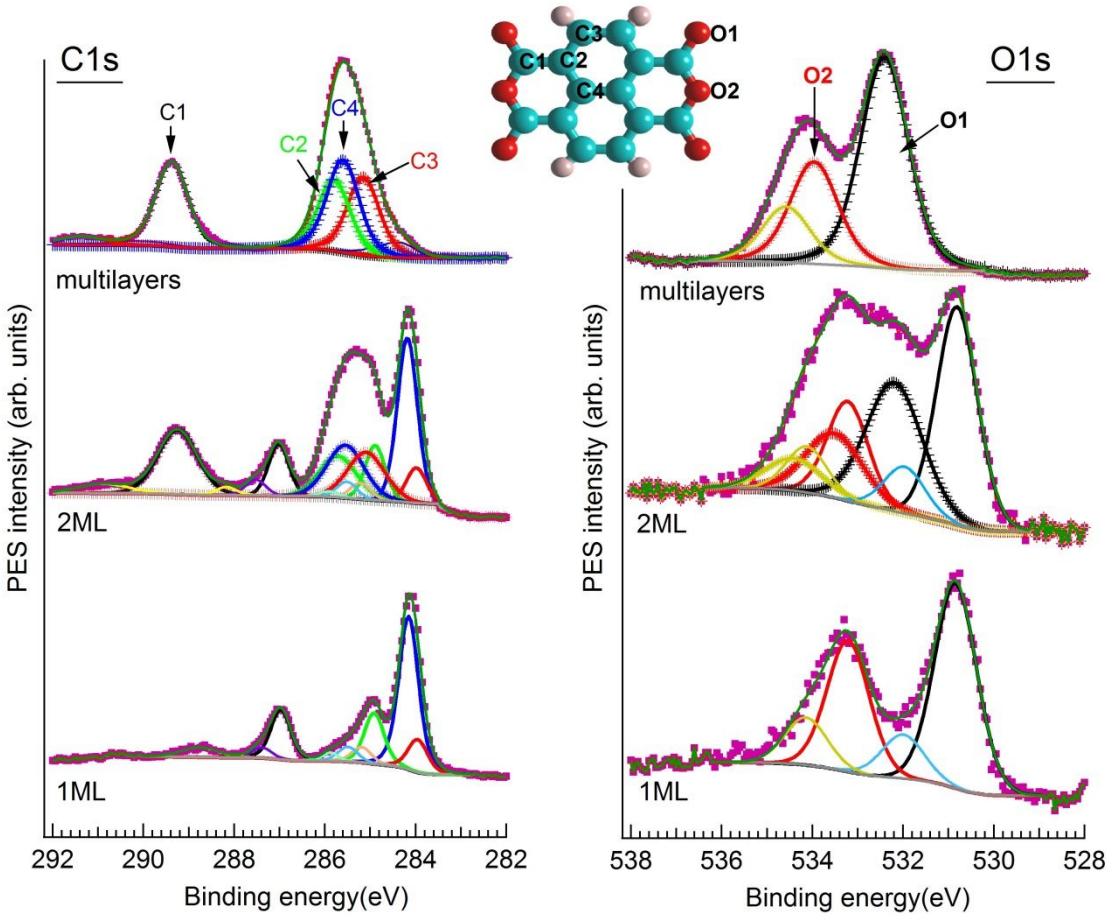

Figure 4: The deconvolution of the C1s (a) and O1s (b) core level spectra after a Shirley background subtraction. The beam energy was 360eV for C1s and 700eV for O1s measurements.

Due to the existence of four distinguishable C atoms in a single NTCDA molecule (see insert of Figure 4) and also considering the satellite effect, it is not surprising to see a complicated fitting spectrum containing various components. The fitting results are presented in Table 1. Starting from the monolayer spectrum for C1s, the high energy resolution offered at TEMPO beamline allows us to discriminate between the different spectroscopic components.

Figure 5 shows the experimental (top) and the theoretical (bottom) *core level energies* for each O and C component. Although the absolute value of the experimental and theoretical core level energies cannot be compared, the comparison of its relative position allows to identify the components of the experimental spectra.

The features at 284.9eV, 283.95eV and 284.15eV could be assigned to carbon atoms C2-C4 within the naphthalene core, and the small peaks at 285.47eV, 285.15eV and 285.45eV correspond to their shake-up satellites, respectively. The peak at 286.97eV is associated with the anhydride carbon and its satellites are located at higher energy in the range of 287-290eV. The spectrum is rather different for the multilayer system, in which only two predominant peaks at 285.6eV and 289.35eV prevail. The former could be reasonably fitted with three components (color marked lines) corresponding to the C2-C4 atoms of the naphthalene core, while the latter is related to the anhydride carbon. The 2ML spectrum was given as an intermediate state. It contains two C1 atom signals coexisting at 289.25eV and 287.0eV, corresponding to the C1 atoms of the multilayer phase and of the monolayer system, respectively. Similarly, the C2-C4 signals are presented in the fitting results with marked lines (multilayer) and solid lines (monolayer). The voigt line-width used for the fitting was 0.5 eV in the monolayer spectrum and 0.7 eV in the multilayer. These two values were also applied in the intermediate phase spectrum (2ML). Some points worth noting in the intermediate phase are: first, compared to the multilayer case, the C2-C4 components from the second monolayer show a tiny shift of less than 0.1eV in binding energy, which could result from the band bending effect that acting on the variation of the work function. Second, the splitting between the C1 and C2-C4 peak becomes larger from 2.82eV in the monolayer to the value of 3.75eV in the multilayer. This significant difference, of almost 1 eV, clearly indicates a strong covalent bonding between the anhydride groups and the substrate, rather than the bonding between the naphthalene core and the Ag substrate. Interestingly, the 2ML system, presents a splitting of also 3.7eV for the second monolayer and 2.83eV for the first monolayer. This reveals that the second monolayer presents already similar characteristics as the multilayer case.

Table 1: Core level energy positions from the fitting at different coverages

	Carbon	Binding energy (eV)	Oxygen	Binding energy (eV)
First ML	C1	286.97	O1	530.85
	C2	284.90	O2	533.20
	C3	283.95	S1	531.99
	C4	284.15	S2	534.14
	S1	287.37		
	S2	285.85		
	S3	285.15		
	S4	285.45		
Second ML	C1	289.25	O1	532.20
	C2	285.70	O2	533.55
	C3	285.10	S	534.45
	C4	285.55		
	S1	290.80		
	S2	288.50		
	S3	287.50		
	S4	288.10		
Thick Layer	C1	289.35	O1	532.40
	C2	285.80	O2	533.95
	C3	285.15	S	534.55
	C4	285.60		
	S1	291.35		
	S2	288.55		
	S3	287.50		
	S4	288.15		

The fitting of the O1s spectrum is given as complementary information. Considering the fact that there are only two different oxygen atoms, the fitting would be reasonably straightforward. For the monolayer system, the spectrum can be fitted with two main components O1 and O2 at 530.85 eV and 533.20 eV, corresponding to the two different oxygen atoms. Two other satellite structures were added at 532 eV and 534.14 eV to well simulate the fitting of the spectrum. The multilayer spectrum has a similar shape and can be fitted with two predominant peaks at 532.4 eV, 533.95 eV corresponding to the different oxygen species and with another peak at 534.55 eV, which is associated with a shake-up satellite. For the 2 ML system, one observes similar behavior as for the

C1s. One should put two different sets of components to well reproduce the 2 ML spectrum. The two sets of components correspond to the one monolayer and the multilayer peaks.

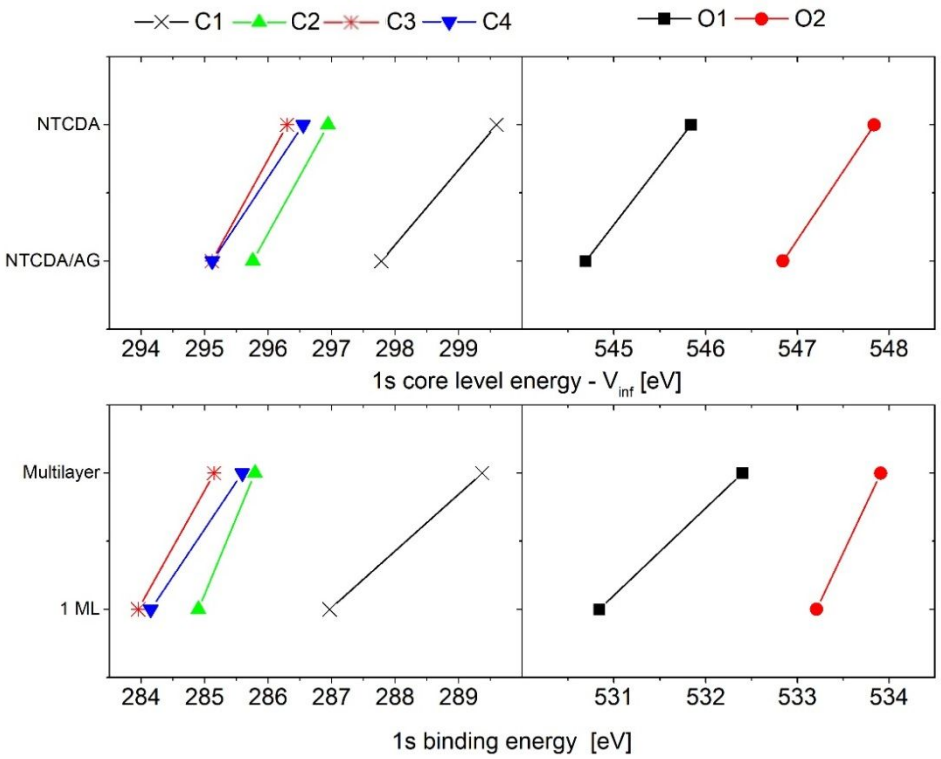

Figure 5: Experimental (bottom) and theoretical (top) energy of the O1s (left) and C1s (right) core level. The NTCDA scheme describes the atom numbering.

3.3. Valence band

UPS measurements have been conducted to investigate the electronic properties close to the Fermi level. Figure 6a shows valence band data obtained on NTCDA films at different thicknesses taken at low photon energy of 60 eV. The Ag(110) valence band is also shown for the comparison.

One can see a predominant intensity in the 4-8 eV range, which originates from the Ag 4d-bands. Upon deposition of NTCDA, the intensity of such bands is significantly reduced, in particular after deposition of a thick layer. At higher binding energies, several resonances develop and become predominant at the multilayer coverage, referring to the orbitals localized within the NTCDA molecules. Additional features occur in the lower binding energy part, close to the Fermi level. These structures are well seen in Figure 6b. Unlike the Cu(100) case where the Cu 3d-bands overlap with the molecular orbital structures, for the present system one observes the appearance of three new features.

The calculated total density of states DOS (Figure 6c) shows the same features experimentally observed. In this figure it is well seen that the structures observed around the Fermi energy come from molecular states. A Bader analysis shows a charge transfer of 1.23 electrons from the surface to the molecule resulting in a partial occupied LUMO, appearing in the spectra as the feature located at around 0.5 eV, which is cut by the Fermi level. The larger width of the LUMO with

respect to the other lower energy structures is due to a higher hybridization with the surface. The other two structures located at around 3.4 eV and 2.5 eV correspond to the HOMO-1, and HOMO of the NTCDA molecules and the projected DOS (Figure 6d) shows that these structures have mainly sp^2 and p_z character respectively. Such features have also been observed for NTCDA on other metal surfaces[52,53] and also for the case of PTCDA/metal systems.[54,55]

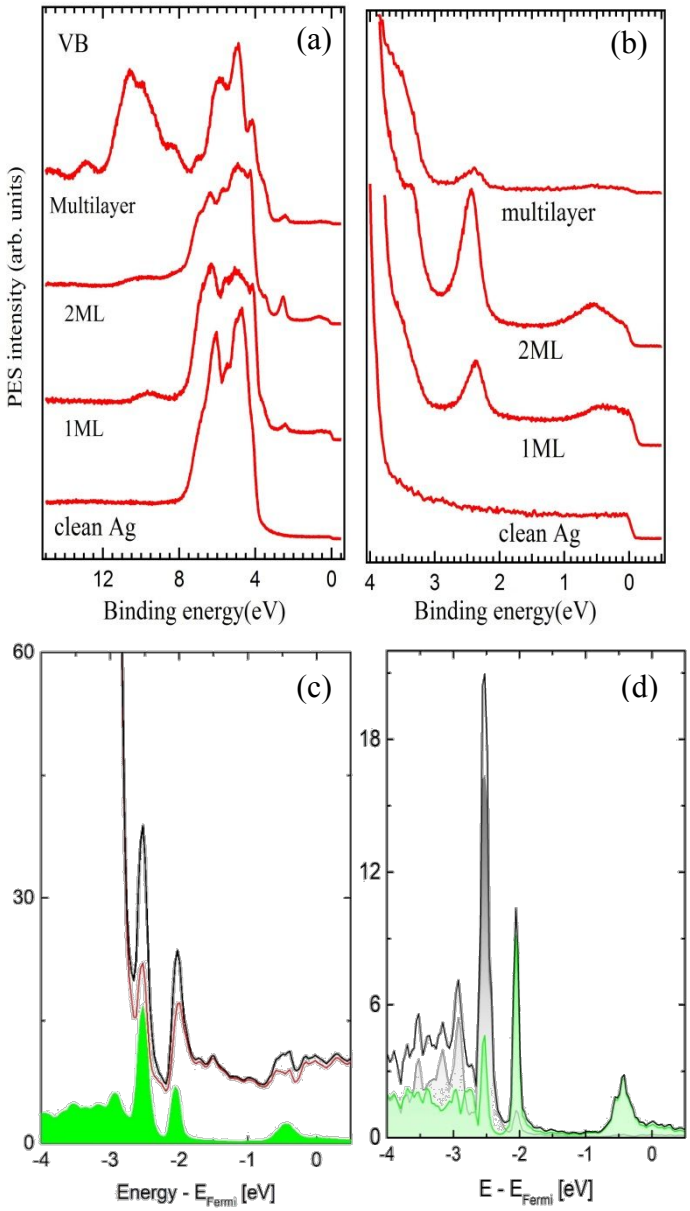

Figure 6: (a) UPS spectra of the NTCDA films at different thicknesses on Ag(110) taken at 60eV beam energy; (b) zoom of the valence band in the range between 0-4eV, showing the HOMO-1, HOMO and F-LUMO. The clean Ag spectrum is also given for comparison. (c) Calculating DOS: total for NTCDA/Ag(110) (black line); projected on Ag atoms (red line), and projected on NTCDA molecule (green fill contour); (d) Projected DOS of NTCDA/Ag(110) on NTCDA: total (black line); pz character (green fill contour) and sp2 character (grey line).

3.4. NEXAFS analysis

NEXAFS measurements have been performed here to probe the molecular orientation at different NTCDA thicknesses. Figure 7a depicts the C K-edge adsorption spectrum, which consists of π* resonances in the 284-292 eV range and a σ* resonance at higher photon energy.[56] The π* orbital, which lies perpendicular to the molecular plane, is probed through the excitation of C1s electrons into the LUMO (LUMO+1) final state. By varying the angle of the incident beam, the π* resonance shows a clear angular dependence behavior, indicating an ordered arrangement of the NTCDA monolayer.

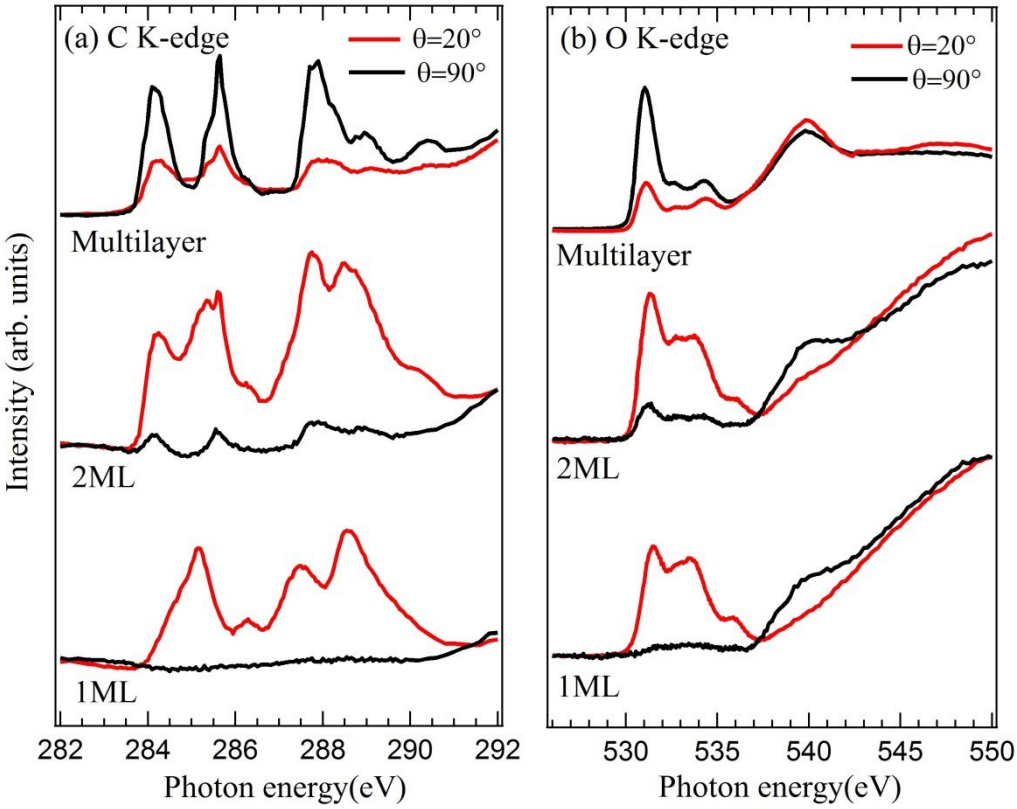

Figure 7: (a) Angular dependence of the C K-edge NEXAFS of NTCDA at different coverages. The Spectra show the π resonance in the range of 282-292eV. (b) O K-edge NEXAFS at the corresponding coverage. The angle θ in the spectra refers to the angle of the in-coming beam with respect to the surface plane.*

We start from the multilayer spectrum as it has a better resolution with predominant resonances compared to the others. The multilayer spectrum consists of resonances located at 284.1 eV, 285.6 eV, 287.9 eV, and 288.8 eV. The first two resonances correspond to the excitation of C1s electron to the LUMO and LUMO+1 within the naphthalene core and the other two relate to the anhydride ones[56]. While in the 2 ML and 1 ML spectra, the four resonances are less resolved due to the strong influence from the Ag coupling (mainly because the π* orbitals of the aromatic ring are involved in the bonding to the Ag substrate). What we would like to highlight here is the angular dependence behavior of the NEXAFS spectra. For the 1ML system, one can notice that at normal incidence of the beam, the adsorption resonances are strongly reduced while at grazing incidence, the intensity

reached the maximum. The O K-edge adsorption spectra given in Figure 7b show the same behavior. Considering that the photon beam is 100% linearly polarized, one reaches the conclusion that at 1 ML coverage the NTCDA molecules are lying down on the surface. At thick layer, an opposite effect is observed indicating that the molecules are standing-up. For the 2 ML system, a quantitative analysis of the C K-edge spectrum at grazing configuration (θ=20°) is shown in Figure 8. The spectrum is fitted as $I(E) = \alpha * I^{1ML}_{\theta=20°} + \beta * I^{2ML}_{\theta=20°}$. It reveals a large NEXAFS signal (grey area) originating from molecules of the first monolayer ($\alpha = 0.6$), while the rest stems from weakly bonded molecules in the second monolayer ($\beta = 0.4$), since the corresponding NEXAFS curve (green area) resembles much to the one of thick layer, but with molecules lying flat because the measurements were made at grazing incidence. This signifies that most of the molecules in the second monolayer are flat-lying and have a weak interaction with the substrate. On the other hand, one observes some weak resonances at the normal incidence configuration (Figure 7a, 2ML, θ=90°), which means that there are also NTCDA molecules with standing-up orientation. All this indicates that within the 2ML films, the first monolayer is lying down while the second monolayer presents a mixed molecule orientation; flat-lying and standing-up.

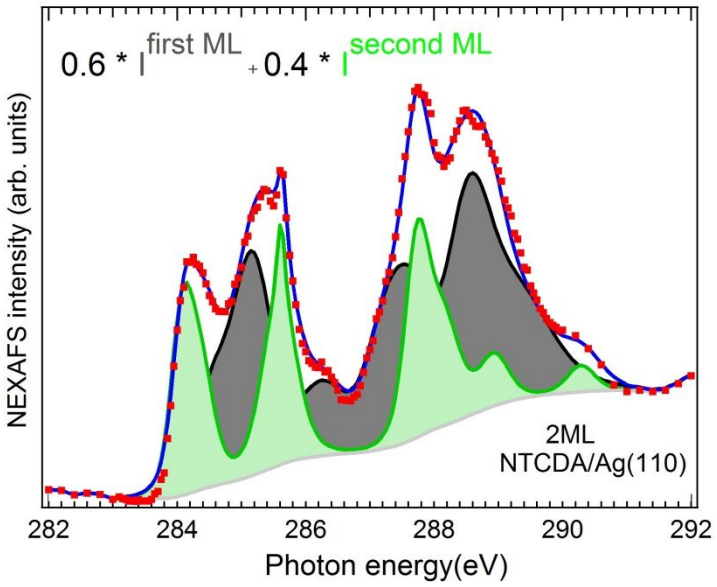

Figure 8: Quantitative analysis of the C K-edge NEXAFS spectrum taken at grazing incidence configuration on 2 ML of NTCDA on Ag(110).

5. Conclusion

In this study a combination of LT-STM, LEED, and photoemission measurements with DFT calculations was made to investigate the structural and chemical properties of NTCDA layers deposited on Ag(110). The unit cell with respect to the Ag(110) lattice was inferred from the LEED, and a molecular arrangement was proposed with the molecule axis parallel to the [001] substrate direction. High resolution LT-STM results further confirmed the existence of two domains with a clear boundary line and where the orbitals within the naphthalene core are well resolved. A detailed description of the molecular orientation within each domain was derived from DFT

calculations, obtaining a good agreement between simulated and experimental STM images. This allowed a better insight of the molecular arrangement. Using photoemission, we have analysed the C1s core level spectra and identified the different chemical environments of the carbon atoms within the molecules. The interface interaction was probed by UPS, which shows the presence of a partially filled LUMO feature induced by a charge transfer process from the Ag substrate into the LUMO of the molecule. Finally, NEXAFS shows a clear angular dependence, indicating a well ordered monolayer with a lying-down structure. The less resolved features in the NEXAFS spectra compared to the gas phase molecules can be a hint of strong coupling between the Ag electronic states and the NTCDA molecular orbitals. To confirm this new theoretical description of the NTCDA/Ag(110) monolayer configuration we also describe the XPS, UPS experimental with theoretical results.

References

1. Barth, J. V., Molecular Architectonic on Metal Surfaces. *Annu. Rev. Phys. Chem.* **2007**, *58*, 375-407.
2. Forrest, S. R., Ultrathin Organic Films Grown by Organic Molecular Beam Deposition and Related Techniques. *Chem. Rev.* **1997**, *97*, 1793-1896.
3. Forrest, S. R.; Leu, L.Y.; So, F.F.; Yoon, W.Y. Optical and Electrical Properties of Isotype Crystalline Molecular Organic Heterojunctions. *J. Appl. Phys.* **1989**, *66*, 5908.
4. Hirose, Y.; Kahn, A.; Aristov, V.V.; Soukiassian, P.; Bulovic, V.V.; Forrest, S. R. Chemistry and Electronic Properties of Metal-Organic Semiconductor Interfaces: Al, Ti, In, Sn, Ag, and Au on PTCDA. *Phys. Rev. B: Condens. Matter. Mater. Phys.* **1996**, *54*, 13748.
5. Moons, E. Conjugated Polymer Blends: Linking Film Morphology to Performance of Light Emitting Diodes and Photodiodes. *J. Phys.: Condens. Matter* **2002**, *14*, 11235.
6. Cicoira, F.; Santato, C. Organic Light Emitting Field Effect Transistors: Advances and Perspectives. *Adv. Funct. Mater.* **2007**, *17*, 3421-3434.
7. Barraud, C.; Seneor, P.; Mattana, R.; Fusil, S.; Bouzehouane, K.; Deranlot, C.; Graziosi, P.; Hueso, L.; Bergenti, I.; Dediu, V.; et al. Unravelling the Role of the Interface for Spin Injection into Organic Semiconductors. *Nat. Phys.* **2010**, *6*, 615-620.
8. Blom, P.W.M.; Mihailetchi, V.D.; Koster, L.J.A.; Markov, D.E. Device Physics of Polymer: Fullerene Bulk Heterojunction Solar Cells. *Adv. Mater.* **2007**, *19*, 1551-1566.
9. Brabec, Ch. J.; Sariciftci, N.S.; Hummelen, J.C. Plastic Solar Cells. *Adv. Funct. Mater.* **2001**, *11*, 15-26.
10. Maruyama, T.; Sugawara, N.; Hirasawa, A.; Akimoto, K. Chemical Bonding and Electronic Properties of NTCDA/Metal Interfaces. *Surf. Sci.* **2001**, *493*, 697-701.
11. Stanzel, J.; Weigand, W.; Kilian, L.; Meyerheim, H.L.; Kumpf, Ch.; Umbach, E. Chemisorption of NTCDA on Ag(1 1 1): a NIXSW Study Including Non-Dipolar and Electron-Stimulated Effects. *Surf. Sci.* **2004**, *571*, L311-L318.
12. Fink, R.; Gador, D.; Stahl, U.; Zou, Y.; Umbach, E. Substrate-Dependent Lateral Order in Naphthalene-Tetracarboxylic Dianhydride Monolayers. *Phys. Rev. B* **1999**, *60*, 2818.
13. Stahl, U.; Gador, D.; Soukopp, A.; Fink, R.; Umbach, E. Coverage-Dependent Superstructures in Chemisorbed NTCDA Monolayers: a Combined LEED and STM Study. *Surf. Sci.* **1998**, *414*, 423-434.
14. Gador, D.; Buchberger, C.; Fink, R; Umbach, E. Manipulation of Molecular Orientation in Ultrathin Organic Films: NTCDA on Ag(111). *Europhys. Lett.* **1998**, *41*, 231.
15. Ueno, N.; Kera, S. Electron Spectroscopy of Functional Organic Thin Films: Deep Insights Into Valence Electronic Structure in Relation to Charge Transport Property. *Prog. Surf. Sci.* **2008**, *83*, 490 -557.
16. Kakuta, H.; Toru, H.; Matsuda, I.; Nagao, T.; Hasegawa, S.; Ueno, N.; Sakamoto, K. Electronic Structures of the Highest Occupied Molecular Orbital Bands of a Pentacene Ultrathin Film. *Phys. Rev. Lett.* **2007**, *98*, 247601.
17. Brédas, J.-L.; Beljonne, D.; Coropceanu, V; Cornil, J. Charge-Transfer and Energy-Transfer Processes in π-Conjugated Oligomers and Polymers: A Molecular Picture. *Chem. Rev.* **2004**, *104*, 4971-5004.

18. Stadler, C.; Hansen, S.; Schöll, A.; Lee, T-L.; Zegenhagen, J.; Kumpf, C.; Umbach, E.; Molecular Distortion of NTCDA Upon Adsorption on Ag(111): a Normal Incidence X-Ray Standing Wave Study. *New J. Phys.* **2007**, *9*, 50.
19. Ziroff, J.; Hame, S.; Kochler, M.; Bendounan, A.; Schöll, A.; Reinert, F. Low-Energy Scale Excitations in the Spectral Function of Organic Monolayer Systems. *Phys. Rev. B: Condens. Matter Phys.* **2012**, *85*, 161404.
20. Bendounan, A.; Aït-Ouazzou, S. Role of the Shockley State in Doping of Organic Molecule Monolayer. *J. Phys. Chem. C* **2016**, *120*, 11456−11464.
21. Jia, J.; Esaulov, V. A.; Bendounan, A. Adsorption and Desorption Kinetics of NTCDA Molecules on Ag(111) and Au(111) Surfaces Studied by Ion Scattering. *Radiat. Eff. Defects Solids* **2017**, *172*, 39-47.
22. Li, K.-S.; Chang, Y.-M.; Agilan, S.; Hong, J.-Y.; Tai, J.-C.; Chiang, W.-C.; Fukutani, K.; Dowben, P. A.; Lin, M.-T. Organic Spin Valves with Inelastic Tunneling Characteristics. *Phys. Rev. B* **2011**, *83*, 172404.
23. Azuma, Y.; Akatsuka, S.; Okudaira, K. K.; Harada, Y.; Ueno, N. Angle-Resolved Ultraviolet Photoelectron Spectroscopy of In-[Perylene-3,4,9,10-Tetracarboxylic Dianhydride] System. *J. Appl. Phys.* **2000**, *87*, 766-769.
24. Shen, Z.; Burrows, P. E.; Bulović, V.; Forrest, S. R.; Thompson, M. E. Three-Color, Tunable, Organic Light-Emitting Devices. *Science* **1997**, *276*, 2009–2011.
25. Ostrick, J. R.; Dodabalapur, A.; Torsi, L.; Lovinger, A. J.; Kwock, E. W.; Miller, T. M.; Galvin, M.; Berggren, M.; Katz, H. E. Conductivity-Type Anisotropy in Molecular Solids. *J. Appl. Phys.* **1997**, *81*, 6804–6808.
26. Kilian, L.; Hauschild, A.; Temirov, R.; Soubatch, S.; Schöll, A.; Bendounan, A.; Reinert, F.; Lee, T. –L.; Tautz, F. S.; Sokolowski, M.; et al. Role of Intermolecular Interactions on the Electronic and Geometric Structure of a Large π-Conjugated Molecule Adsorbed on a Metal Surface. *Phys. Rev. Lett.* **2008**, *100*, 136103-136106.
27. Adachi, M.; Murata, Y.; Nakamura, S. Spectral Similarity and Difference of Naphthalenetetracarboxylic Dianhydride, Perlenetetracarboxilic Dianhydride, and Their Devrivatives. *J. Phys. Chem* **1995**, *99*, 14240-14246.
28. Serkovic Loli, L. N.; Sánchez, E. A.; Esteban Gayone, J.; Grizzi, O.; Esaulov, V. A. Assembly and Thermal Stability of Thin EP-PTCDI Films on Ag(111). *Phys. Chem. Chem. Phys.* **2009**, *11*, 3849–3853.
29. Sauvage-Simkin, M.; Coati, A.; Garreau, Y.; Vlad, A.; Müller, K.; Bendounan, A.; Kara, A. In-Depth Atomic Structure of the Pentacene/Cu(110) Interface in the Monolayer Coverage Regime: Theory and X-Ray Diffraction Results. *J. Phys. Chem. C* **2014**, *118*, 27815-27822.
30. Scheybal, A.; Müller, K.; Bertschinger, R.; Wahl, M.; Bendounan, A.; Aebi, P.; Jung, T. A. Modification of the Cu(110) Shockley Surface State by an Adsorbed Pentacene Monolayer. *Phys. Rev. B* **2009**, *79*; 115406-115411.
31. Braatz, C. R.; Esat, T.; Wagner, C.; Temirov, R.; Tautz, F. S.; Jakob, P. Switching Orientation of Adsorbed Molecules: Reverse Domino on a Metal Surface. *Surf. Sci.* **2016**, *643*, 98-107.
32. Rosenow, P.; Jacob, P.; Tonner, R. Electron−Vibron Coupling at Metal−Organic Interfaces from Theory and Experiment. *J. Phys. Chem. Lett.* **2016**, *7*, 1422-1427.
33. Tonner, R.; Rosenow, P.; Jakob, P. Molecular Structure and Vibrations of NTCDA Monolayers on Ag(111) From Density-Functional Theory and Infrared Absorption Spectroscopy. *Phys. Chem. Chem. Phys.* **2016**, *18*, 6316-6328.
34. Falkenberg, Ch.; Uhrich, Ch.; Olthof, S.; Maenning, B.; Riede, M. K.; Leo, K. Efficient p-i-n Type Organic Solar Cells Incorporating 1,4,5,8-Naphthalenetetracarboxylic Dianhydride as Transparent Electron Transport Material. *J. Appl. Phys.* **2008**, *104*, 034506-034511.
35. Burtman, V.; Zelichenok, A.; Yitzchaik, S. Organic Quantum—Confined Structures Though Molecular Layer Epitaxy. *Angew. Chem. Int. Ed.* **1999**, *38*, 2041-2045.
36. Walzer, K.; Maennig, B.; Pfeiffer, M.; Leo, K. Highly Efficient Organic Devices Based on Electrically Doped Transport Layers. *Chem. Rev.* **2007**, *107*, 1233−1271.
37. Kresse, G.; Hafner, J. Ab Initio Molecular Dynamics for Liquid Metals. Phys. Rev. B **1993**, *47*, 558 - 561.
38. Kresse, G.; Hafner, J., Ab Initio Molecular-Dynamics Simulation of the Liquid-Metal–Amorphous-Semiconductor Transition in Germanium. *Phys. Rev. B* **1994**, *49*, 14251 - 14269.
39. Blöchl, P. E.; Projector Augmented-Wave Method. *Phys. Rev. B* **1994**, *50*, 17953 - 17979.
40. Perdew, J. P.; Wang, Y. Accurate and Simple Analytic Representation of the Electron-Gas Correlation Energy. *Phys. Rev. B* **1992**, *45*, 13244 -13249.

41. Dion, M.; Rydberg, H.; Schröder, E.; Langreth, D. C.; Lundqvist, B. I. Van der Waals Density Functional for General Geometries. *Phys. Rev. Lett.* **2004**, *92*, 246401.
42. Román-Pérez, G.; Soler, J. M. Efficient Implementation of a van der Waals Density Functional: Application to Double-Wall Carbon Nanotubes. *Phys. Rev. Lett.* **2009**, *103*, 096102.
43. Monkhorst, H. J.; Pack, D. Special Points for Brillouin-Zone Integrations. *Phys. Rev. B* **1976**, *13*, 5188 - 5192.
44. Methfessel, M.; Paxton, A. T. High-precision Sampling for Brillouin-Zone Integration in Metals. *Phys. Rev. B* **1989**, *40*, 3616 – 3621.
45. Henkelman, G.; Arnaldsson, A.; Jónsson, H. A Fast and Robust Algorithm for Bader Decomposition of Charge Density. *Comput. Mater. Sci.* **2006**, *36*, 354-360; Sanville, E.; Kenny, S. D.; Smith, R.; Henkelman, G. Improved Grid-Based Algorithm for Bader Charge Allocation. *J. Comp. Chem.* **2007**, *28*, 899 - 908.
46. Tersoff, J.; Hamann, D.R. Theory of the Scanning Tunneling Microscope. *Phys. Rev. B* **1985**, *31*, 805 - 813.
47. Strohmeier, R.; Ludwig, C.; Petersen, J.; Gompf, B.; Eisenmenger, W. STM Investigations of NTCDA on Weakly Interacting Substrates. *Surf. Sci.* **1996**, *351*, 292-302.
48. Strohmeier, R.; Petersen, J.; Gompf, B.; Eisenmenger, W. A Systematic STM Study of Planar Aromatic Molecules on Inorganic Substrate: I. Submolecular Image Contrast. *Surf. Sci.* **1998**, *418*, 91-104.
49. Tong, Y.; Nicolas, F.; Kubsky, S.; Oughaddou, H.; Sirotti, F.; Esaulov, V.; and Bendounan, A. Interplay between Structural and Electronic Properties in 1,4,5,8-Naphthalenetetracarboxylic Dianhydride Films on Cu(100). *J. Phys. Chem. C* **2017**, *121*, 5050-5057.
50. Abbasi, A.; Scholz, R. Ab Initio Calculation of the Dispersion Interaction Between a Polyaromatic Molecules and a Noble Metal Substrate: PTCDA on Ag(110). *J. Phys. Chem. C* **2009**, *113*, 19897-19904.
51. Weissner, M.; Kübert, J.; Feyer, V.; Puschnig, P.; Schöll, A.; Reinert, F. Lateral Band Formation and Hybridization in Molecular Monolayers: NTCDA on Ag(110) and Cu(100). *Phys. Rev. B* **2013**, *88*, 075437.
52. Mura, M.; Gulans, A.; Thonhauser, T.; Kantorovich, L. Role of van der Waals Interaction in Forming Molecule-Metal Junctions: Flat Organic Molecules on the Au(111) Surface. *Phys. Chem. Chem. Phys.* **2010**, *12*, 4759-4767.
53. Maruyama, T.; Hirasawa, A.; Shindow, T.; Akimoto, K.; Kato, H.; Kakizaki, A. Energy-Level Alignment at NTCDA/Metal and PTCDA/NTCDA Interfaces Studies by UPS. *J. Lumin.* **2000**, *87-89*, 782-784.
54. Ziroff, J.; Forster, F.; Schöll, A.; Puschnig, P.; Reinert, F. Hybridization of Organic Molecular Orbitals with Substrate States at Interfaces: PTCDA on Silver. *Phys. Rev. Lett.* **2010**, *104*, 233004.
55. Duhm, S.; Gerlach, A.; Salzmann I.; Bröker, B.; Johnson, R.L.; Schreiber, F.; Koch, N. PTCDA on Au(111), Ag(111) and Cu(111): Correlation of Interface Charge Transfer to Bonding Distance. *Org. Electron.* **2008**, *9*, 111-118.
56. Bendounan, A.; Forster, F.; Schöll, A.; Batchelor, D.; Zirrof, J.; Umbach, E.; Reinert, F. Electronic Structure of 1 ML NTCDA/Ag(111) Studied by Photoemission Spectroscopy. *Surf. Sci.* **2007**, *601*, 4013-4017.

TOC graphic